buildings

MDPI

Article

Progressive-Collapse Mechanism of Suspended-Dome Structures Subjected to Sudden Cable Rupture

Zhenyu Xu [1,*] and Shen Yan [1,2]

[1] College of Civil Engineering, Tongji University, Shanghai 200092, China; s.yan@tongji.edu.cn
[2] State Key Laboratory of Disaster Reduction in Civil Engineering, Tongji University, Shanghai 200092, China
* Correspondence: xuzhenyusd@126.com

Abstract: This article proposes an progressive-collapse mechanism for suspended-dome structures subjected to cable rupture, based on experimental and finite element results. The anti-collapse mechanism can be succinctly described as a node-buckling mechanism: the potential for node buckling in a local arch-like spatial grid centered on unsupported node directly determines whether progressive collapse will occur in the overall structure. Subsequently, based on this anti-collapse mechanism, a node-buckling model is further proposed, and the factors affecting the anti-collapse bearing capacity of suspended domes are quantitatively expressed through the construction of a resistance index, which can be used to judge the sensitivity of hoop cables. Further, using Ribbed and Lamella suspended domes as examples, extensive calculations demonstrate the applicability and accuracy of the node-buckling model and resistance index to other types of suspended domes. Finally, the resistance index is used to analyze two important but easily overlooked factors that affect the anti-collapse bearing capacity of suspended domes. Initial geometric imperfections result in a rise–span ratio too small for the local arch-like spatial grid, while the lack of lateral stiffness at the supports will weaken the axial stiffness of the outermost radial or diagonal members. Both of these factors significantly reduce the stability of the local arch-like spatial grid, making it more likely to trigger progressive collapse in suspended-dome structures.

Keywords: suspended-dome structures; cable rupture; progressive collapse; node-buckling model; resistance index; initial geometric imperfections; support lateral stiffness

Citation: Xu, Z.; Yan, S. Progressive-Collapse Mechanism of Suspended-Dome Structures Subjected to Sudden Cable Rupture. *Buildings* **2023**, *13*, 1533. https://doi.org/10.3390/buildings13061533

Academic Editor: Krishanu Roy

Received: 16 May 2023
Revised: 12 June 2023
Accepted: 13 June 2023
Published: 15 June 2023

1. Introduction

The progressive collapse of structures refers to the phenomenon wherein a local failure, usually induced by unexpected load, promotes the continuous propagation of the failure and causes a partial or complete collapse of the structure that is disproportionate to the initial failure. Currently, research on the progressive collapse of frame structures is relatively mature, and relevant standards and guidelines have been proposed and revised [1–4]. There has also been substantial progress in the research on the progressive collapse of rigid spatial structures, and researchers have conducted progressive collapse tests, numerical simulations, and theoretical analyses of rigid spatial structures, such as trusses [5–7], single-layer latticed domes [8–10], and grid frames, and have proposed corresponding anti-collapse mechanisms. However, research on the progressive collapse of composite flexible–rigid spatial structures is still in the exploration stage. A suspended dome is a typical rigid–flexible composite space structure that combines the benefits of cable domes and single-layer latticed domes. They are widely used in large-scale public buildings, such as stadiums and convention centers, because of their high rigidity, good stability, and ease of construction. Each cable, which serves as the main structural component, can withstand extremely high tensile forces. When external reasons cause the failure of a cable or its anchorage, it leads to a large range of tension system relaxation, which could eventually cause the entire structure to collapse progressively. As a flexible member,

the dynamic response of the cable during the initial failure and subsequent failure are completely different from those of a rigid member. Therefore, the structural response, local failure propagation process, and anti-collapse mechanism are obviously different from that of a frame structure or rigid spatial structure, and they must be studied separately.

Thus far, there has been little research on the progressive collapse of suspended-dome structures. Zhang et al. [11] employed numerical simulations to show that the failure of hoop cables and columns is vulnerable to progressive collapse, whereas the failure of struts, diagonal cables, and upper reticulated dome members has little impact on the overall structure. Qu et al. [12] performed the numerical simulation of progressive collapse with respect to an actual suspended-dome structure and demonstrated the failure of the support system will cause excessive local deformation and even local failure of the structure. Wang et al. [13] conducted a dynamic-impact-effect experiment on a suspended-dome structure subjected to hoop-cable rupture and obtained the response of the structural members. Liu et al. [14] undertook a comparative FE analysis of the collapse resistance of Levy-type and loop-free suspended dome following accidental cable failure. It was concluded that the loop-free suspended dome displays superior collapse resistance, and identified that the most critical cable is located in the outermost layer of the cable–strut system. The occurrence of progressive collapse was found to depend on the bearing capacity of the reticulated shell and the residual contribution of the cable–strut system. Zhao et al. [15] conducted a progressive collapse test on a Kiewit suspended-dome model with a diameter of 4.2 m and revealed the structural response and the local failure propagation process of suspended-dome structures subjected to initial local failure.

In summary, the current research on the progressive collapse of suspended-dome structures primarily relies on numerical simulations or collapse tests. However, these studies often focus on specific suspended-dome structures, and their conclusions may lack generalizability. Moreover, previous research has primarily emphasized the dynamic response of suspended-dome structures during progressive collapse, with little investigation into the anti-collapse mechanisms and the factors influencing the anti-collapse bearing capacity of suspended-dome structures.

In this study, a progressive collapse numerical simulation was initially carried out for a suspended-dome structure, building upon the progressive collapse test [15] and using a validated numerical simulation method. This led to the proposal of an anti-collapse mechanism for the suspended-dome structure in the event of a ruptured hoop cable. Subsequently, the node-buckling model and the calculation method of the resistance index were introduced, based on the anti-collapse mechanism. These can be utilized to assess the sensitivity of the hoop cable and quantitatively evaluate factors that influence the anti-collapse capacity of the suspended-dome structure. Moreover, the accuracy and applicability of the node-buckling model and the resistance index for various types of suspended-dome structures were demonstrated by using Ribbed and Lamella suspended-dome structures as examples. Lastly, using the resistance index as a basis, the effects of two often-overlooked factors—initial geometric imperfections and lateral stiffness of the supports—on the anti-collapse capacity of the suspended-dome structure were analyzed.

2. FE Investigations of Progressive Collapse of Suspended Domes

2.1. Finite Element Method and Its Validation

This section is based on the explicit dynamic finite element program ABAQUS/Explicit [16] used to analyze the dynamic response and collapse process of suspended-domes after hoop-cable failure. Firstly, the test data from Reference [15] is used to verify the FE method used.

The span and rise of the suspended-dome test model were designed to be 4.2 m and 0.6 m, respectively. A K6 Kiewit single-layer latticed dome was constructed from steel pipes with two different cross-sections: the outermost component was subjected to significant force, and there were no struts under the center of the latticed dome. Therefore, all members in the outermost hoop and all members in the innermost hoop were made

entirely of ø12 × 1 mm steel pipe, while the remaining members used ø10 × 1 mm steel pipe. The lower cable–strut system was composed of hoop cables, diagonal cables, and struts: all cables were ø7 mm steel strands, and struts were all made of ø12 × 1 mm steel pipe, with a length of 0.45 m. The suspended-dome structure was installed on the substructure which served as a tensile member to bear the horizontal force of the model and also provide a sufficient clearance during the progressive collapse (Figure 1a). The naming conventions for the nodes, members, and cables in the test model are consistent with those used in the finite element model, as shown in Figure 2.

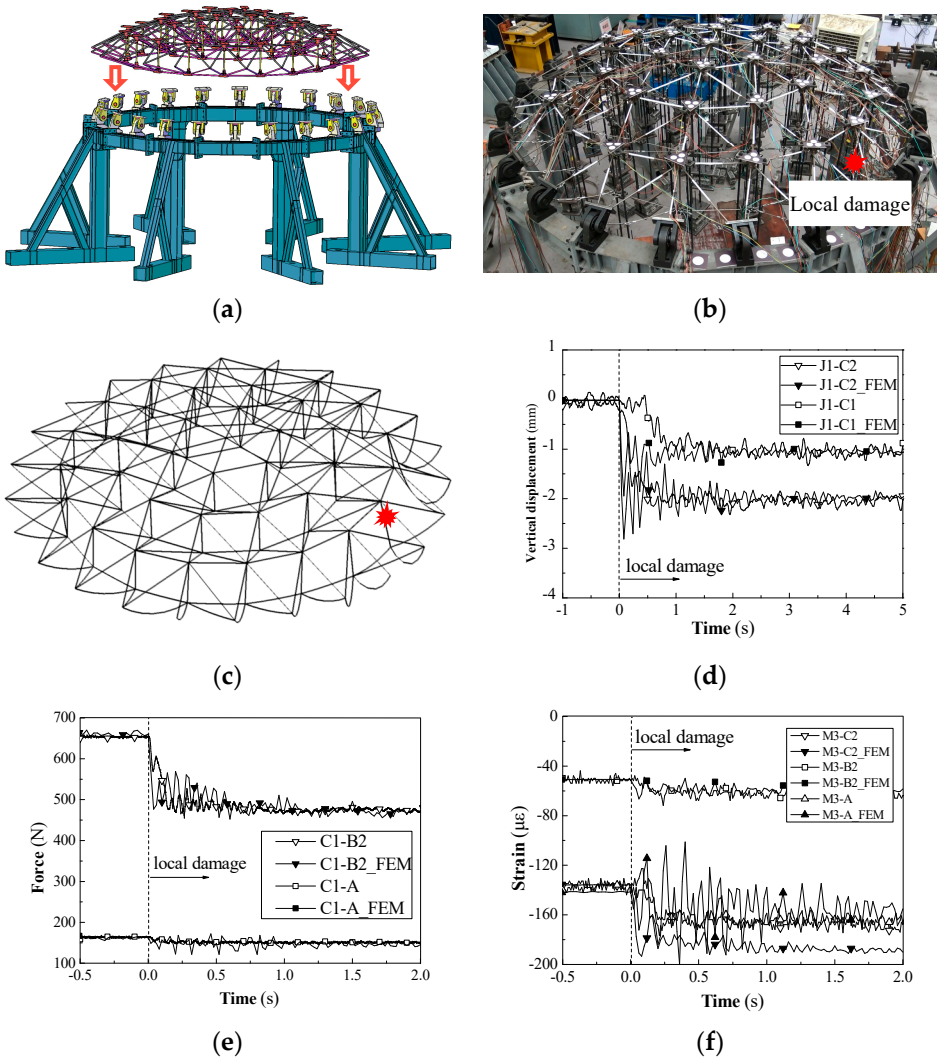

Figure 1. Finite element simulation results for the test. (**a**) Tested suspended-dome model, (**b**) equilibrium geometries of test model, (**c**) equilibrium geometries of FE model, (**d**) vertical displacement, (**e**) cable force, and (**f**) strain responses.

The geometric dimensions, material properties, initial pre-stress, and boundary conditions of the FE model were determined based on the actual situation of the test. The dome members were modeled with B31 elements (two-node linear space beam element in ABAQUS), while the cable was modeled with T3D2 elements (two-node linear three-dimensional truss element in ABAQUS). The lattice-shell members were rigidly connected, and the struts were hinged with the lattice shell and the cables. The uniformly distributed roof loads were simplified as vertical point loads at all nodes, which were modelled with lumped masses. The equivalent temperature-lowering method was adopted for the pre-tension of the cable, and the element deletion proposed in the literature [6] was used to simulate the failure of the cable.

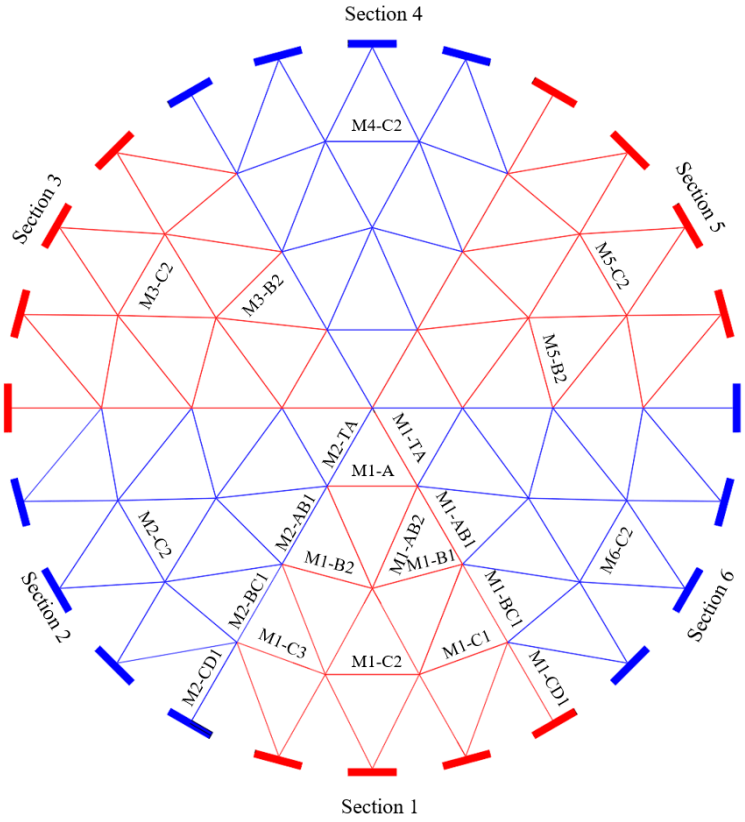

(**a**)

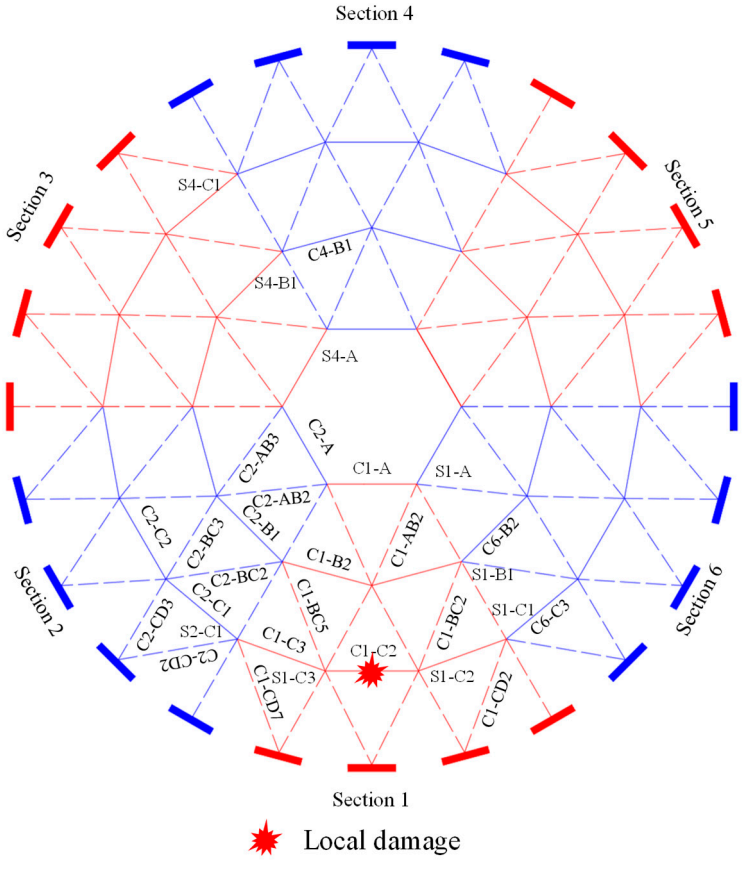

(**b**)

Figure 2. Suspended-dome model. (**a**) The upper lattice shell, and (**b**) the cable–strut system.

The FE results Indicate that after the failure of the outer hoop cable (C1-C2), the structure does not collapse, and a new tension system is formed at the outer hoop cable, which is highly consistent with the test results (Figure 1b,c). The vertical displacement, cable force and strain responses in the FE simulation are in good agreement with the test results (Figure 1d–f). Therefore, the FE method used in this study can accurately predict the response of the remaining structure after cable rupture in suspended-domes.

2.2. Suspended-Dome Analysis Model

The FE analysis model should take a suspended-dome structure, which is closer to the actual large-span roof structure, as the research object. The overall size of the FE model was 10 times that of the test model [15], and the cross-sectional dimensions of the dome members and cable were adjusted after 10-times magnification to meet the common specifications of steel pipes and steel strands. The K6-4 Kiewit latticed dome, with a diameter of 42 m and rise of 6 m, was adopted to model the upper part of the suspended-dome structure. The lower part of the dome was equipped with a three-layer cable–strut system, and the height of the strut was 4.5 m. All members except cables were constructed using steel pipes and had two different cross-sections: ø168 × 5 mm was adopted for the hoop, radial, and diagonal members of the outermost and innermost hoop, while ø159 × 5 mm was adopted for the others. The cables were 6 × 7ø5 mm steel strands. The mechanical properties of the members are listed in Table 1. The pre-tension forces of the hoop cables from the inner to outer hoops were 20, 70, and 140 kN, respectively.

Table 1. Mechanical properties of suspended-dome members.

Members	Elastic Modulus (MPa)	Yield Strength f_y (MPa)	Ultimate Strength f_y (MPa)
Steel pipe	2.06×10^5	320	420
Steel strand	1.67×10^5	/	1570

The roof load includes a dead load of 0.8 kN/m^2 and live load of 0.5 kN/m^2. The partial load factor is also taken as the value of the dynamic nonlinear analysis in the DoD2009 Anti-collapse Design Specification [3]: G = 1.2 DL + 0.5 LL = 1.21 kN/m^2. The authors of [15] confirmed that when the roof load is set to G = 1.21 kN/m^2, the suspended-dome structure will not undergo progressive collapse. Therefore, the roof load was increased to 1.6 G = 1.936 kN/m^2 to explore the anti-collapse mechanism of the suspended-dome structure.

The test model was divided Into six Identical sector partitions, with the mesh In each sector partition surface divided according to the principle of equal length of radial members on the horizontal projection plane. The nodes, latticed dome members, and cables were labeled in each section, as shown in Figure 2. The common members in Zone 1 can be considered as an example to demonstrate the numbering principle, and the remaining nodes, members, and cables are numbered analogously. The label of the latticed dome joint starts with J, and J1-C2 represents the second node from left to right on the third hoop (hoop C) in Zone 1. The label of the cable joint starts with j, and j1-C2 represents the cable joint directly below the latticed dome node J1-C2. The label of the strut starts with S, and S1-C2 connects J1-C2 and j1-C2. The label of the latticed dome member starts with M, where M1-B1 denotes the first hoop member of the second hoop (hoop B) of the latticed dome from left to right, and M1-AB2 denotes the second radial or diagonal latticed dome member between the first and second hoops (hoop A and hoop B) from left to right. The label of the cable starts with C, where C1-B1 denotes the first hoop cable from left to right in the second hoop, and C1-AB2 denotes the second hoop cable from left to right between the first and second hoops.

2.3. Numerical Simulation Results and Anti-Collapse Mechanism

Numerical simulation results show that when the roof load is increased to 1.6 G, after the rupture of C1-C2 hoop cable, the initial failure expands progressively, ultimately

leading to the overall collapse of the structure. The progressive collapse process is shown in Figure 3. Figure 4a displays the displacement time history of the nodes in the lattice shell, revealing that the collapse extends from the outer hoop to the middle and inner hoops, and from the initial failure position to both sides.

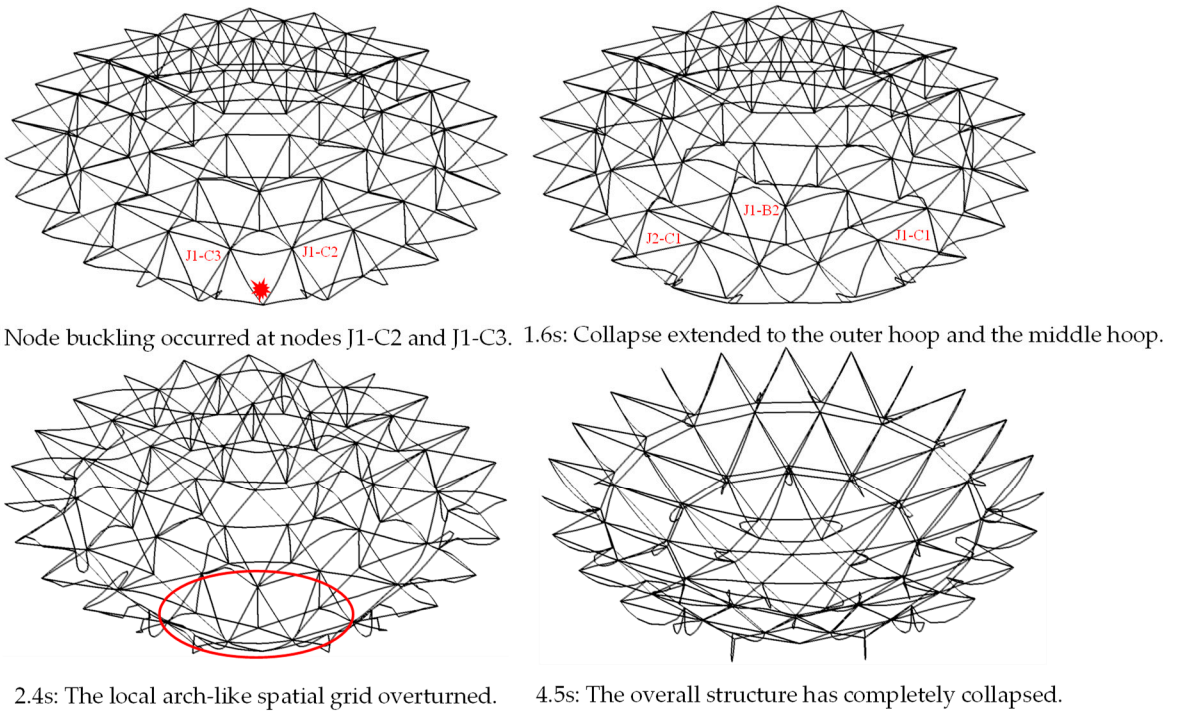

Figure 3. Collapse process of the suspended-dome model under a roof load of 1.6 G.

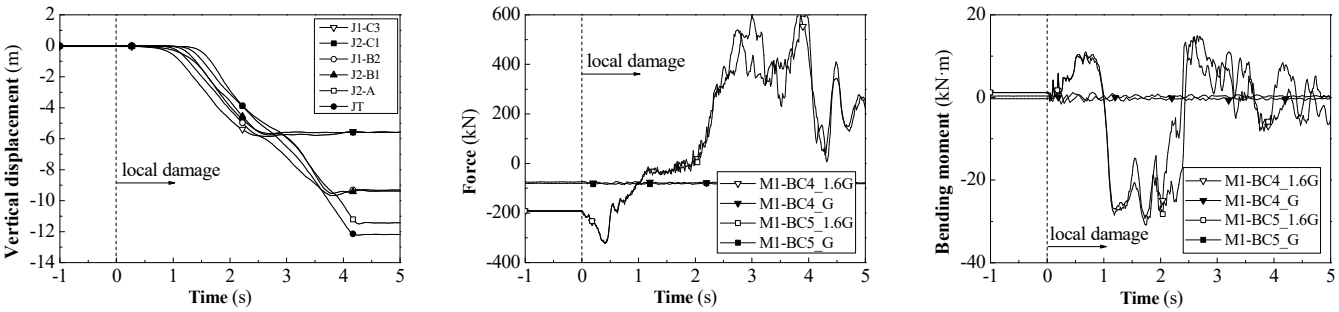

Figure 4. Time history of the suspended-dome structure under a roof load of 1.6 G. (**a**) Vertical displacement, (**b**) axial force in the diagonal members, and (**c**) bending moment in the diagonal members.

The collapse started above the ruptured hoop cable C1-C2, with the local arch-like spatial grid (with J1-C2 and J1-C3 as vertices and the connecting members as bracing rods) at the vertices J1-C2 and J1-C3 experiencing "node buckling" [6] first, characterized by a rapid change in the axial force and bending moment within the local arch-like spatial-grid members, as shown in Figure 4b,c. Taking the diagonal member M1-BC4 as an example, after the failure of C1-C2, due to the loss of the support of strut S1-C3, the axial compression force within M1-BC4 rapidly increased to 320 kN within 0.5 s, and then quickly decreased with the occurrence of node buckling, completing a snap-through change from compression to tension, with the maximum axial tensile force reaching 600 kN. Before the failure of C1-C2, the lattice-shell members mainly bore axial forces, and the bending moments at the ends were not significant. After the failure of C1-C2, the bending moment within M1-BC4 rapidly increased, and the upper surface of the lower end cross-section was subjected to

tension while the lower surface was subjected to compression. Subsequently, the bending moment within the member reversed as node buckling was completed. In contrast, in the structure with a roof load set to G, after the failure of C1-C2, the axial forces and bending moments within the diagonal members M1-BC4 and M1-BC5 only slightly increased, and node buckling did not occur at the local arch-like spatial grid.

After the node buckling of the local arch-like spatial grid, the initial failure began to extend to the middle and inner hoops. Owing to the rapid downward movement of nodes J1-C3 and J1-C2, diagonal cables C1-BC2 to C1-BC5 connecting the outer hoop of the latticed dome and middle hoop cable were completely relaxed, resulting in the failure of the middle hoop cable–strut system. In addition to losing the support of strut S1-B2, the middle hoop node J1-B2 was also dragged downward by the diagonal members M1-BC3 and M1-BC4 and finally started to fall swiftly. Based on the same principle, the initial failure spread from the outer hoop to the middle hoop and then to the inner hoop.

Numerical simulation results show that the failure of the outer hoop cable caused the corresponding upper lattice-shell nodes to lose the support of the struts, becoming unsupported nodes. The unsupported nodes rely on the local arch-like spatial grid centered on itself to resist external loads. Comparing the dynamic responses of structures under two different loads, it can be found that whether the local arch-like spatial grid can resist external loads through internal force redistribution will directly determine if the overall structure undergoes progressive collapse. If the bearing capacity of the local arch-like spatial grid is higher than the external loads, it can maintain balance by utilizing the arching and bending mechanisms of the local arch-like spatial grid. Once the bearing capacity of the local arch-like spatial grid is lower than the external load, node buckling similar to snap-through buckling will occur at the unsupported node, which is the direct cause of progressive collapse in suspended-dome structures.

3. Resistance Index Based on Node Buckling

3.1. Node-Buckling Model

The unsupported node and the local arch-like spatial grid are extracted to construct the node-buckling model; the node-buckling model mainly consists of the upper lattice shell, and the influence of the cable–strut system on the upper lattice shell needs to be considered. Before the initial damage occurs, the cable–strut system can be divided into the support effect of the struts and the circumferential stiffness provided by the self-balancing system. For a complete structure, the shell nodes are still supported by the struts in the vertical direction; the far end of the connected members is supported by the struts, and the axial direction is constrained by the self-balancing system. Therefore, the boundary condition at the far end of the members can be simplified as hinged. At this time, the struts and cable–strut system work together to balance the vertical load P. The simplified calculation model of the complete structure is shown in Figure 5.

When the hoop cable fails, the nodes above the failed cable segment lose the support of the struts and rely solely on the cable–strut system to resist external loads. Therefore, the struts are removed in the node-buckling model, leaving only the cable–strut system. It should be noted that the far end of the circumferential members connected to the unsupported nodes also lose the support of the struts, so the circumferential nodes have a tendency to fall simultaneously. Therefore, the effect of the circumferential components is ignored, and the model is reduced to an arch composed of only four oblique members, as shown in Figure 6.

3.2. Resistance Index and Its Validation

Section 2.3 highlights that when the hoop cable fails, the lattice-shell nodes above the failed hoop cable lose strut support, becoming unsupported nodes. Consequently, the lattice shell relies on the local arch-like spatial grid centered on the unsupported node to resist the external loads. Therefore, node buckling at the unsupported node will directly determine whether the suspended-dome structure experiences a progressive collapse. Analytical

calculation of the critical buckling load for the node-buckling model is impractical. This section identifies the primary factors affecting node buckling at unsupported nodes and quantitatively expresses the impact of these factors by constructing a resistance index.

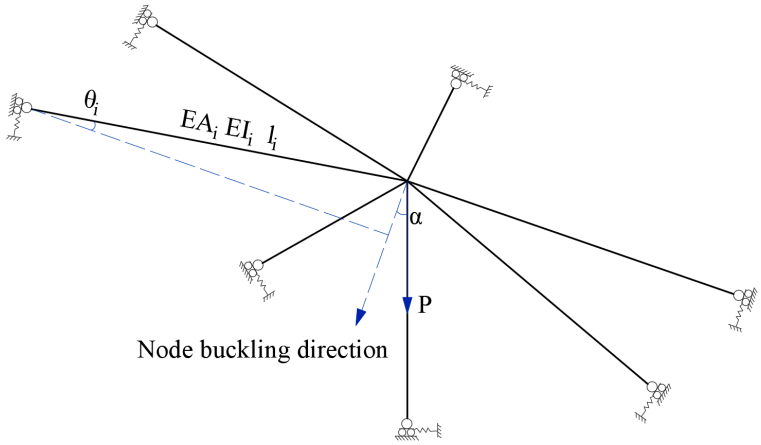

Figure 5. Simplified calculation model of the complete structure.

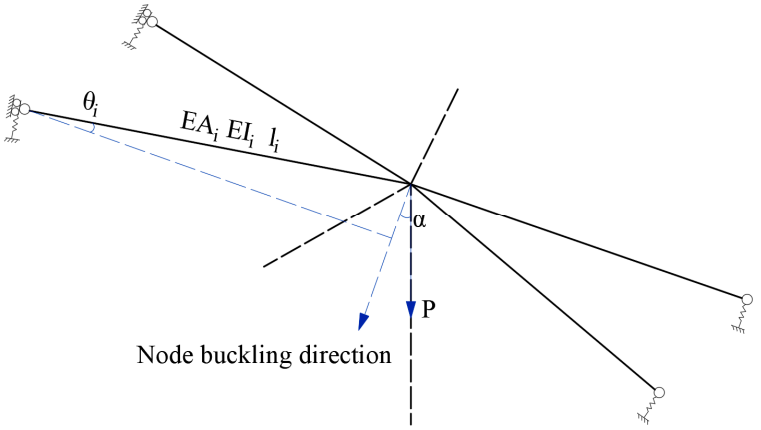

Figure 6. Node-buckling calculation model after hoop-cable failure.

(1) The first parameter f_{p} represents the impact of the vertical load at the unsupported node, which is the direct cause of node buckling. The calculation method, shown in Equation (1), represents the external load P component along the node-buckling direction, where α is the angle between the load direction, normally vertical, and the node-buckling direction, approximately towards the center of the spherical dome, as shown in Figure 5. That is, nodes closer to the bottom have more vertical external load components acting on the stiffer spherical dome, causing less impact on node buckling perpendicular to the spatial grid. A larger f_{p} value indicates a greater load perpendicular to the local arch-like spatial grid at the unsupported node, increasing the likelihood of node buckling.

$$f_{\mathrm{P}} = P \cdot \cos(\alpha) \tag{1}$$

(2) The second parameter f_{k} represents the stiffness characteristics of the members connected to the unsupported node. Obviously, when the member stiffness increases, the out-of-plane stiffness of the local arch-like spatial grid also increases. F_{k} can be characterized as the sum of the stiffness of each member in the node-buckling direction, including axial stiffness and bending stiffness, as shown in Equation (2). The larger the f_{k}, the greater the stiffness of the local arch-like spatial grid, and the more advantageous it is to avoid node buckling.

$$f_{\mathrm{K}} = \sum\left(\frac{EA^i}{l^i}\sin^2\left(\theta^i\right) + \frac{3EI^i}{\left(l^i\right)^3}\cos^2\left(\theta^i\right)\right) \tag{2}$$

where the term in the bracket is the stiffness of a tilting member I, with one end fixed and the other end pinned, in the node-buckling direction; E is the modulus of elasticity, A^i is the cross-sectional area, I^i is the second moment of area of the cross-section, l^{i} is the member length, and θ^i is the tilting angle, as shown in Figure 5.

(3) The third parameter f_{R} represents the impact of the cable–strut system failure range. A larger range covered by the failed hoop cable and fewer distributed struts negatively affect the structure's anti-collapse performance. F_{R} depends on two factors: the area covered by the failed hoop cable A_{N} and the total number of struts at the failed hoop-cable location S_{N}. Since the total number of struts is related to the hoop-cable perimeter, f_{R} can be represented as shown in Equation (3), where r represents the radius covered by the corresponding hoop cable. A larger f_{R} value indicates a smaller failure range, making it more advantageous to avoid node buckling.

$$f_{\mathrm{R}} = \frac{A_n}{S_n} = \frac{1}{r} \tag{3}$$

In summary, the critical load for node buckling due to hoop-cable failure can be expressed in the form of the resistance index *R.I.*, as shown in Equation (4). A smaller *R.I.* for a cable segment signifies higher structural sensitivity to initial failure, increasing the likelihood of progressive collapse. When the hoop cable fails, the resistance index should be calculated for both nodes above the hoop cable, with the minimum value serving as the resistance index for that cable segment.

$$R.I. = \frac{f_{\mathrm{K}} \cdot f_{\mathrm{R}}}{f_{\mathrm{P}}} = \frac{\sum\left(\frac{EA^i}{l^i}\sin^2\left(\theta^i\right) + \frac{3EI^i}{\left(l^i\right)^3}\cos^2\left(\theta^i\right)\right)}{P \cdot r \cdot \cos(\alpha)} \tag{4}$$

Taking the suspended-dome model in Section 2.2 as an example, we evaluate the sensitivity of the cable segments using the resistance index and compare the results with numerical simulations. As shown in Table 2, there is a high degree of consistency between the numerical simulation results and the sensitivity calculations derived from the resistance index. The numerical simulation results reveal that the structure is most sensitive to the initial failure of the outer hoop-cable segment C1-C1. When the equivalent uniformly distributed roof load reaches 1.75 kN/m^2, the failure of segment C1-C1 triggers a progressive collapse of the structure. Moreover, the initial failure of the outer hoop-cable segment C1-C2 is also prone to causing progressive collapse, with a critical collapse load of 1.90 kN/m^2. In contrast, the critical collapse load for the middle hoop-cable segment C1-B1 failure increases to 2.85 kN/m^2, while the failure of the inner hoop-cable segment C1-A1 does not lead to a progressive collapse of the structure. The calculations derived from the resistance index also indicate that the *R.I.* of the outer hoop-cable segment C1-C1 is the lowest, with the *R.I.* increasing progressively from the outer hoop to the inner hoop. This evidence confirms the accuracy of utilizing the resistance index to identify the sensitivity of the cable segments within Kiewit suspended-dome structures.

Table 2. Identification of critical cables in a Kiewit suspended dome.

Cable	FE Simulation		Resistance Index		
	Critical Load (kN/m^2)	Buckling Node	No.	*R.I.*/*R.I.*max	Buckling Node
C1-C1	1.75	C1	1	0.32	C1
C1-C2	1.90	C2, C3	2	0.38	C2, C3

Table 2. *Cont.*

Cable	FE Simulation		Resistance Index		
	Critical Load (kN/m^2)	Buckling Node	No.	*R.I.*/*R.I.*max	Buckling Node
C1-B1	2.85	B2	3	0.61	B2
C1-A1	-	-	4	1	A1

4. Applicability to Other Types of Suspended-Dome Structures

The buckling-mode model and resistance index are not only applicable for explaining the anti-collapse mechanism of Kiewit suspended-dome structures, but are also suitable for other types of suspended-dome structures. The resistance index can be used to assess the sensitivity of hoop cables in suspended-dome structures. In this section, we perform numerical simulations and resistance-index calculations for Ribbed and Lamella suspended-dome structures with hoop-cable failures. Both of these types of suspended-dome structures are widely used in actual structures. The upper shell of the Ribbed suspended-dome structure is composed of quadrilateral grids, which can be used to test the applicability of the resistance-index method for determining sensitive cable segments in suspended-dome structures with non-triangular grids.

In the numerical simulation calculations of this section, some simplifications have been made, as the focus is on the judgment of hoop-cable sensitivity rather than the dynamic response of the structure. The failure time of the initial members is set to 0.1 s, as the structural dynamic response after the hoop-cable breakage converges irrespective of the failure time and damping effect. Therefore, the damping effect is not considered during the calculations. The boundary conditions for all structural models adopt fixed hinged supports, and the influence of initial defects is not considered. As for the determination of progressive collapse, it is assumed that as long as a local arch-like spatial grid is completely overturned, the structure is considered to have undergone progressive collapse.

4.1. Ribbed Suspended-Dome Structure

The diameter of the calculation model for the Ribbed suspended dome was 40 m, and the rise–span ratio was 1/5. The number of longitudinal and latitudinal members in the lattice shell was 30 and 7, respectively; the longitudinal members were also divided according to the equal arc length method. The lower part of the dome was equipped with a six-layer cable–strut system, and the height of the strut was 4.5 m, as shown in Figure 7. There were two types of member cross-sections: longitudinal members M-DE1, M-EF1, and M-FG1 used ø108 × 4 mm, while the remaining longitudinal members, all latitudinal members and struts used ø89 × 4 mm. The cables were 6 × 7ø5 mm steel strands. The mechanical properties of the members were the same as the model in Section 2.2. The pre-tension forces of the hoop cables from the inner to outer were 20, 40, 80, 120, 160, and 220 kN, respectively.

The numerical simulation results (Figure 8) show that the node-buckling mechanism is still applicable to the Ribbed suspended-dome structure. Taking the removal of the outer hoop cable as an example, after the outer hoop-cable segment c-F1-F2 fails, the relaxation of the outer hoop cable leads to the failure of the outer hoop struts. The nodes F1 and F2 lose the support of the struts and experience downward vertical displacement, meaning nodes F1 and F2 undergo node buckling first. The collapse then extends to the remaining outer hoop nodes and neighboring middle-hoop nodes near F1 and F2, eventually causing the complete overturning of the entire structure.

In terms of cable sensitivity, the numerical simulation results are highly consistent with the resistance index, as shown in Table 3. The numerical results show that the structure is most sensitive to the initial failure of the outer hoop-cable segment c-F1-F2. When the equivalent uniformly distributed roof load is 1.50 kN/m^2, the failure of c-F1-F2 triggers the progressive collapse of the structure. The member sensitivity decreases from the outer hoop to the inner hoop, and the critical load causing the structure collapse increases

accordingly. The calculation results of the resistance index also show that the *R.I.* of c-F1-F2 is the lowest, and the *R.I.* increases from the outer hoop to the inner hoop. This confirms the feasibility of using the resistance index to determine sensitive cables for the Ribbed suspended-dome structure.

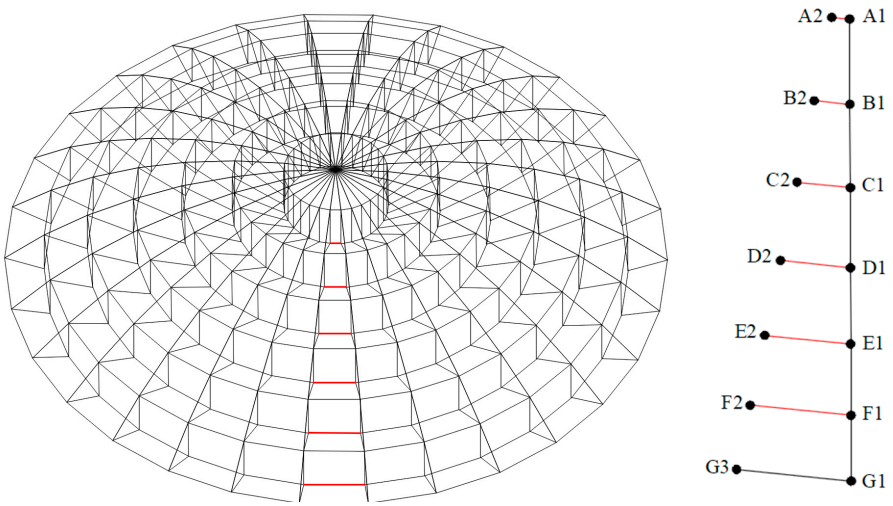

Figure 7. Ribbed suspended-dome structure.

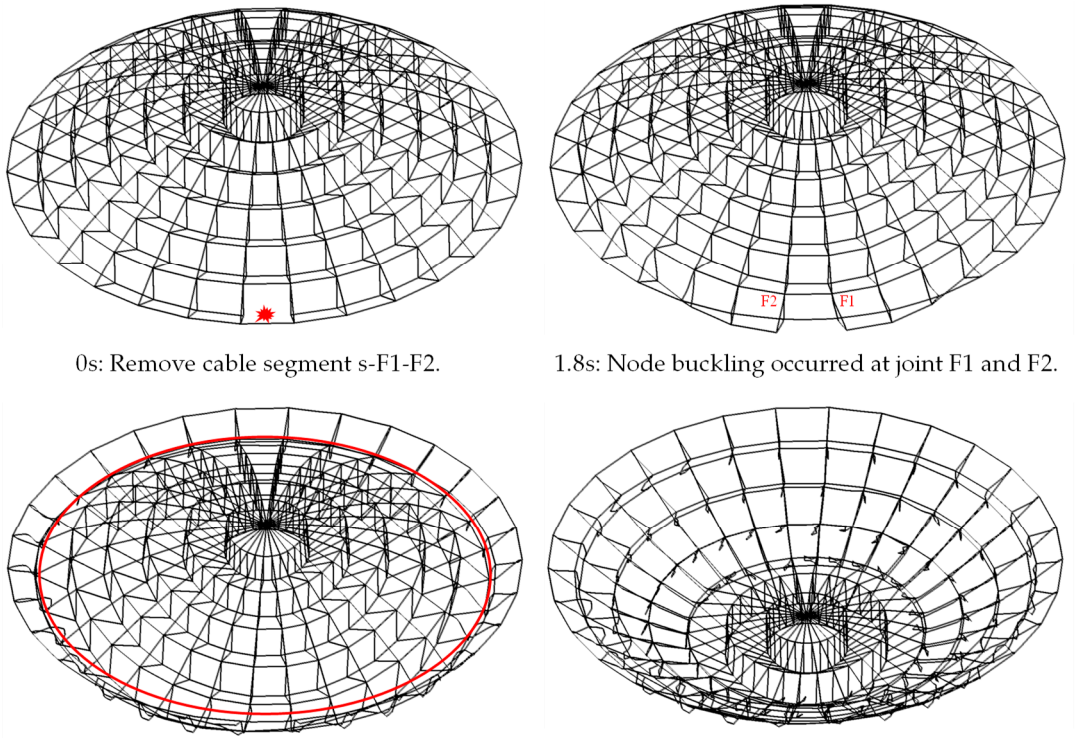

Figure 8. Collapse process of the Ribbed suspended-dome structure.

Table 3. Identification of critical cables in a Ribbed suspended dome.

Cable	FE Simulation			Resistance Index		
	Critical Load (kN/m^2)	Criticality Grade	Buckling Node	No.	*R.I.*/*R.I.*max	Buckling Node
c-F1-F2	1.50	I	F1, F2	1	0.12	F1, F2

Table 3. *Cont.*

Cable	FE Simulation			Resistance Index		
	Critical Load (kN/m^2)	Criticality Grade	Buckling Node	No.	*R.I.*/*R.I.*max	Buckling Node
c-E1-E2	2.25	II	E1, E2	2	0.23	E1, E2
c-D1-D2	2.75	III	D1, D2	3	0.31	D1, D2
c-C1-C2	3.50	IV	C1, C2	4	0.56	C1, C2
c-B1-B2		-	-	5	0.84	B1, B2
c-A1-A2		-	-	6	1	A1, A2

4.2. Lamella Suspended-Dome Structure

The Lamella suspended-dome structure calculation model also used a 40 m span, a 1/5 rise–span ratio, and 7 latitudinal member series. There were 30 nodes on each latitudinal member series, meaning there were 30 left-slanting and 30 right-slanting members in each layer. The lower part of the dome was equipped with a six-layer cable–strut system, and the height of the strut was 4.5 m, as shown in Figure 9. All members had a ø108 × 4 cross-section, and the cables were 6 × 7ø5 mm steel strands. The mechanical properties of the members were the same as the model in Section 2.2. The pre-tension forces of the hoop cables from the inner to outer were 20, 40, 80, 120, 160, and 220 kN, respectively. This type of suspended dome has no longitudinal member series, and can verify the applicability of the sensitivity-judgment method based on the resistance index for suspended domes without longitudinal member series.

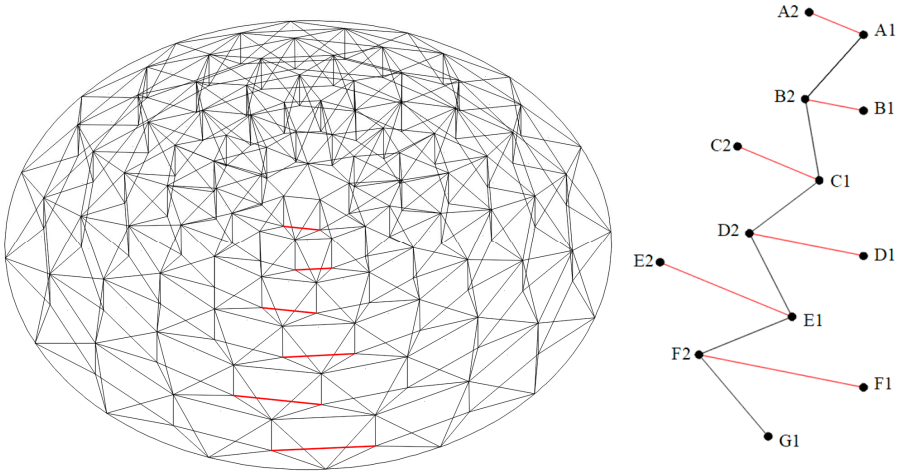

Figure 9. Lamella suspended-dome structure.

The numerical simulation results (Figure 10) show that the node-buckling mechanism is still applicable to Lamella suspended-dome structures. Taking the removal of the outer hoop cable as an example, after the failure of the outer hoop-cable segment c-F1-F2, the relaxation of the outer hoop cable leads to the failure of the outer hoop struts, and the upper nodes F1 and F2 lose the support of the struts, resulting in a downward vertical displacement. Nodes F1 and F2 undergo node buckling first, followed by the collapse of the remaining outer hoop nodes and the middle hoop nodes near F1 and F2, eventually leading to a complete overturning of the whole structure.

In terms of cable sensitivity, the numerical simulation results are highly consistent with the resistance-index results, as shown in Table 4. The numerical results show that the structure is most sensitive to the initial failure of the outer hoop-cable segment c-F1-F2. When the equivalent uniformly distributed roof load is 1.25 kN/m^2, the failure of c-F1-F2 will cause the progressive collapse of the structure. The sensitivity of members decreases from the outer hoop to the inner hoop, and the critical load that causes the collapse of the structure also increases in sequence. The calculation results of the resistance index also

show that the *R.I.* of c-F1-F2 is the lowest, and the *R.I.* increases from the outer hoop to the inner hoop in sequence. This confirms the feasibility of using the resistance index to determine the sensitive members for the Lamella suspended-dome structure.

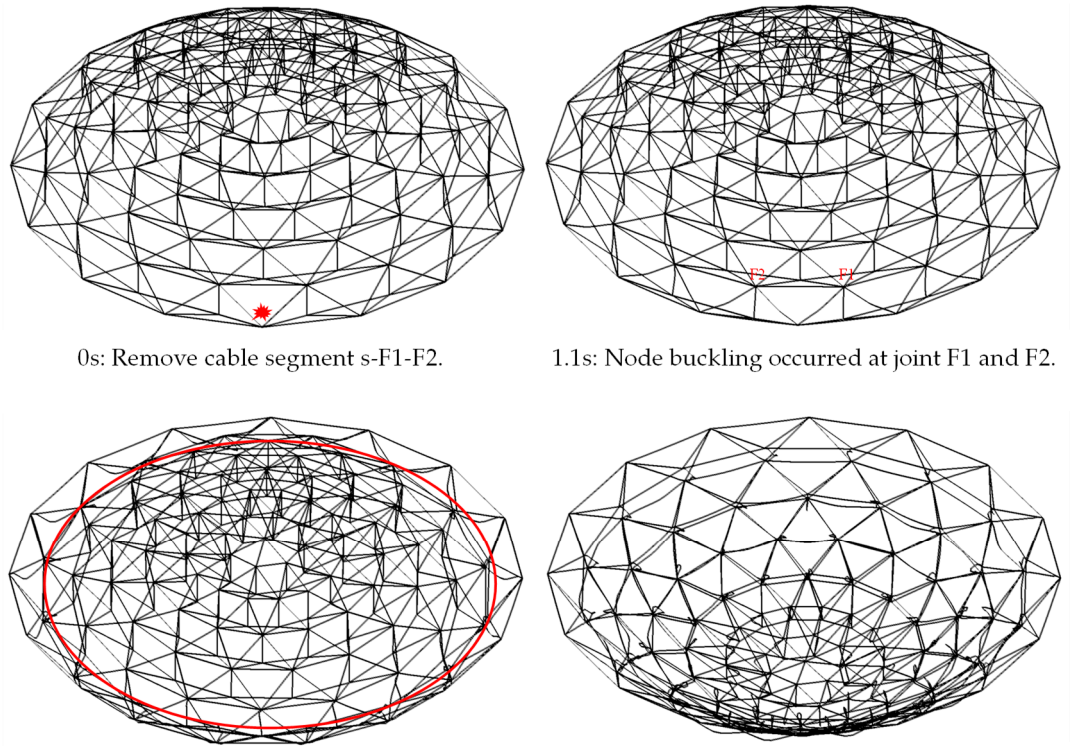

0s: Remove cable segment s-F1-F2. 1.1s: Node buckling occurred at joint F1 and F2.

1.8s: Collapse extended to the outer and middle hoops. 4.0s: The overall structure has completely collapsed.

Figure 10. Collapse process of a Lamella suspended-dome structure.

Table 4. Identification of critical cables in a Lamella suspended dome.

Cable	FE Simulation			Resistance Index		
	Critical Load (kN/m^2)	Criticality Grade	Buckling Node	No.	*R.I.*/*R.I.*max	Buckling Node
c-F1-F2	1.25	I	F1, F2	1	0.11	F1, F2
c-E1-E2	2.00	II	E1, E2	2	0.23	E1, E2
c-D1-D2	2.50	III	D1, D2	3	0.32	D1, D2
c-C1-C2	3.25	IV	C1, C2	4	0.64	C1, C2
c-B1-B2		-	-	5	0.91	B1, B2
c-A1-A2		-	-	6	1	A1, A2

5. Analysis of Influencing Factors on Anti-Collapse Bearing Capacity

Numerous factors affect the anti-collapse bearing capacity of suspended-dome structures. By analyzing the resistance index (*R.I.*), it becomes apparent that for any given suspended-dome structure, the rise–span ratio and the stiffness of the upper shell members have a direct impact on the anti-collapse bearing capacity. For instance, increasing the rise-span ratio of the shell can directly reduce f_{p}, while enhancing the stiffness of the shell members can increase f_{K}. These factors contribute to a notable improvement in the anti-collapse bearing capacity of suspended-dome structures. However, there are two critical factors that significantly influence the anti-collapse bearing capacity of these structures and are not easily derived from formulas. This section will investigate the effects of initial geometric imperfections and the lateral stiffness of supports on the anti-collapse bearing capacity of suspended-dome structures.

5.1. Influence of Initial Geometric Imperfections

The above analysis assumes that the structure is a perfect structure without initial geometric imperfections. Nonetheless, there are inevitably various initial defects in the actual structure, including the overall shape deviation of the curved surface caused by installation errors, initial bending of the member, initial eccentricity of the member to the joint, and initial stress caused by various factors.

The upper single-layer latticed shell of the suspended-dome structure is supported by the lower cable–strut system, which remarkably enhances the stability of the entire structure. Therefore, a complete suspended-dome structure without an initial failure is not sensitive to initial geometric imperfections in its bearing capacity. However, the local suspended-dome structure degenerates into a single-layer latticed dome when initial failure occurs, such as the rapid failure of the hoop cable, which causes the cable–strut system to relax or even fail. In this case, initial geometric imperfections in the upper single-layer latticed dome would significantly reduce its stability.

Assuming that the maximum geometric imperfection occurs at the unsupported node located above the failed hoop cable, a vertical geometric imperfection of 300/L is produced, as illustrated in Figure 11. The initial imperfections predominantly influence the stiffness characteristics f_K of the members connected to the unsupported nodes, wherein f_K is primarily associated with axial stiffness. To simplify calculations, the effects of bending stiffness are disregarded, and it is assumed that the member length l remains constant, with the lengths and cross-sectional dimensions of all members connected to the unsupported nodes being identical.

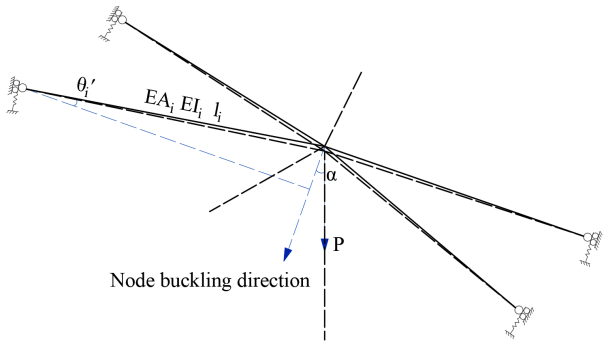

Figure 11. Node-buckling calculation model considering initial geometric imperfections.

At this point, as per Equation (2), the original stiffness characteristic f_K can be simplified to Equation (5). Upon considering the initial imperfections, the stiffness characteristic f'_K is transformed into Equation (6). The weakening coefficient for the structure's collapse bearing capacity after accounting for initial geometric imperfections is represented as d_i, which can be expressed in the form of Equation (7).

$$f_K = \sum\left(\frac{EA^i}{l^i}\sin^2\left(\theta^i\right)\right) \tag{5}$$

$$f\prime_K = \sum\left(\frac{EA^i}{l^i}\sin^2\left(\theta'^i\right)\right) \tag{6}$$

$$d_i = \frac{\sin^2(\theta\prime)}{\sin^2(\theta)} \tag{7}$$

Considering that local arches typically exhibit shallow profiles, the angle θ between the shell members and the spherical direction is generally small. A minor change in θ can result in a substantial alteration in $\sin^2(\theta)$. Using the Kiewit suspended-dome model from Section 2.2 as an example, the initial θ is 0.08 radians. Assuming that the unsupported node generates a 300/L geometric imperfection vertically, A is reduced to 0.05 radians after

accounting for the initial imperfection. The weakening coefficient d_i, as per Equation (7), is calculated to be 0.39. This finding illustrates that, upon considering the initial imperfections, the stability resistance coefficient is reduced to 39% of its original value, highlighting the significant impact of initial imperfections on the anti-collapse bearing capacity of suspended-dome structures.

FE analysis can also be employed to verify the impact of initial imperfections on the anti-collapse bearing capacity of suspended-dome structures. First, eigenvalue buckling analysis was performed for the suspended-dome structure after pre-tension to determine the first-order buckling mode. The initial geometric imperfections of the structure were determined using the consistent mode imperfection method, and the maximum initial defect was considered to be 1/300 (14 cm) of the structural span. Subsequently, the outer hoop cable C1-C2 was removed to obtain the response of the remaining structure.

The failure of the latticed dome started above the failure hoop cable C1-C2, as shown in Figure 12. Figure 13b,c demonstrate that the local arch-like spatial grid (with node J1-C3 as the vertex, M1-BC4, M1-BC5, M1-C3, M1-CD6, M1-CD5, and M1-C2 as the struts) in the structure first suffered "node bucking", which was characterized by a rapid change in the axial force and bending moment in the local arch truss members that first increased and then reversed. After the initial failure of cable C1-C2, strut S1-C3 lost its bearing capacity, resulting in the axial compressive force on diagonal member M1-BC4 rapidly increasing to 220 kN in 0.5 s. With the occurrence of node buckling, the axial force decreased rapidly, completing the jump from compression to tension with a maximum axial tension of 205 kN. After cable C1-C2 failed, the negative bending moment (tension on the upper section, compression on the lower section) in diagonal member M1-BC4 increased rapidly, while it bore little bending moment before failure. Subsequently, with the completion of the local node buckling, the bending moment in the diagonal members was reversed. In contrast, the axial force and bending moment of diagonal members M1-BC4 and M1-BC5 showed no obvious change after the failure of outer hoop cable C1-C2 of the perfect structure without initial geometric imperfections.

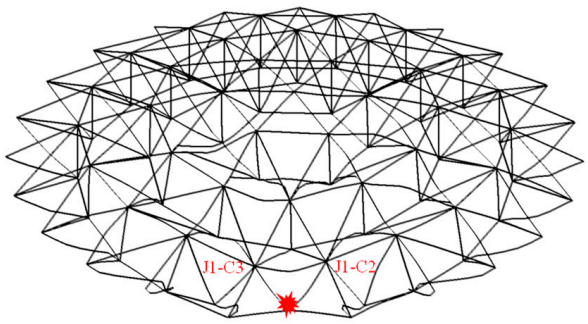

1.0s: Node buckling occurred at joint J1-C2 and joint J1-C3.

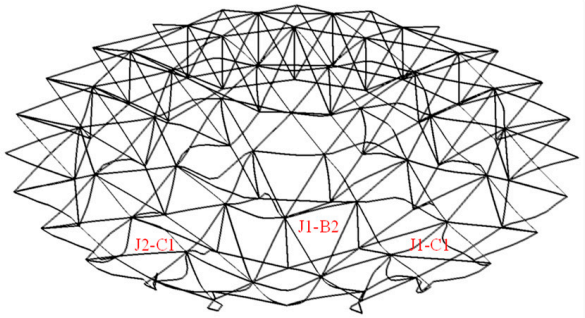

1.8s: Collapse extended to the outer and middle hoops

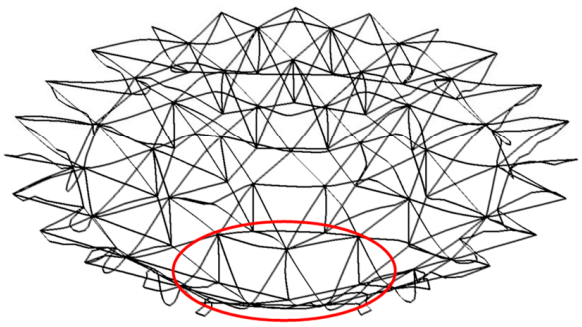

3.0s: The local arch-like spatial grid overturned.

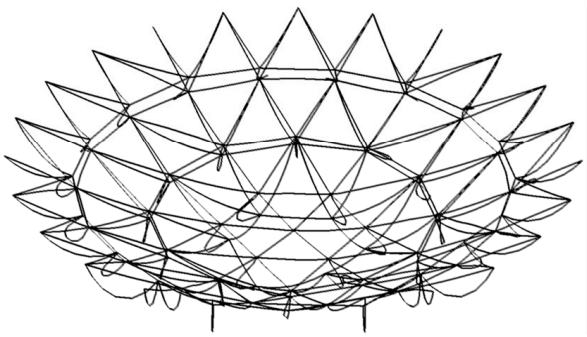

5.0s: The overall structure has completely collapsed.

Figure 12. Collapse process of the suspended-dome structure with initial geometric imperfections.

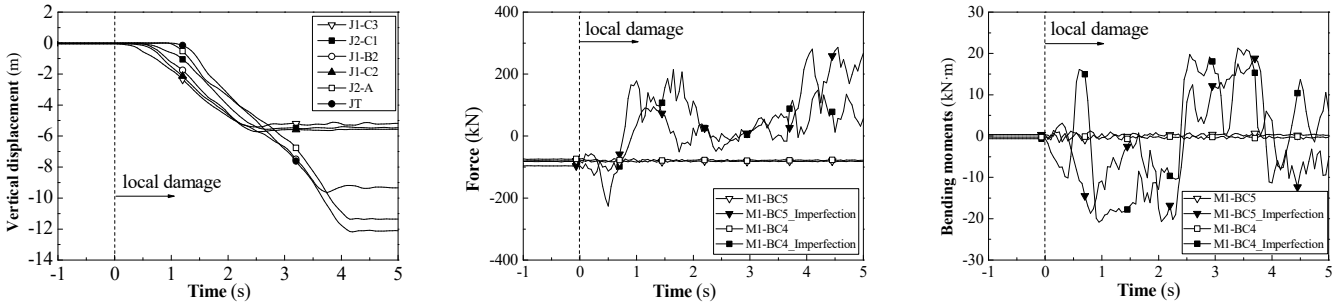

(**a**) (**b**) (**c**)

Figure 13. Time history of the suspended-dome structure with initial geometric imperfections. (**a**) Vertical displacement, (**b**) axial force in the diagonal members, and (**c**) bending moment in the diagonal members.

For a structure without initial geometric imperfections, the equivalent rise (defined as the vertical distance from node J1-C3 to the fitting bottom of the local arch-like spatial grid on node J1-C3) of the local arch-like spatial grid at node J1-C3 is 533 mm, and the rise–span ratio (defined as the ratio of equivalent rise to the distance between nodes J1-C2 and J1-C4) is 1/20. However, for structures with initial flaws, these become 461 mm and 1/24, respectively. As can be observed from the comparison, the rise–span ratio of the structure with initial geometric imperfections has a significant decrease. Additionally, the dynamic effect caused by the failure of cable C1-C2 (mainly reflected in the rapid loss of the bearing capacity of strut S1-C3) magnifies the local roof load, causing node buckling of the node J1-C3, which becomes the primary reason for the progressive collapse of the suspended-dome structure.

In summary, for a suspended-dome structure with initial geometric imperfections, the spatial position of individual nodes is lower than the design value in the vertical direction, which causes a drop in the rise–span ratio of the local arch-like spatial grid with this node as the vertex. When it is the only structure supporting the roof load, a local node buckling of the local arch-like spatial grid can easily occur and then propagate to the adjacent structure, resulting in the progressive collapse of the whole structure.

5.2. Influence of Support Lateral Stiffness

In practical engineering, it is necessary to set up circumferential force-bearing components (ring beams) at the boundary of suspended-dome structures. The base of the ring beam usually adopts two methods: one is a sliding support, allowing the ring beam to slide freely in the radial direction. Limiting devices provide enough sliding distance to release the radial expansion and contraction caused by temperature effects, while preventing the structure from slipping off under earthquake action without horizontal limits. The other method is a fixed hinged support, where the linear displacement of the ring beam is completely constrained. In this case, the tensioning construction needs to be completed before fixing the hinge bearing, avoiding the adverse effects on the ring beam bearing during the cable tensioning process. In the aforementioned analysis, to summarize the anti-collapse mechanism, the influence of the lateral stiffness of the supports was ignored, and only the case with fixed hinged support boundary conditions was considered. However, once the radial constraint is released, the self-balancing system of the structure would be damaged in the event of hoop-cable failure, significantly reducing the anti-collapse bearing capacity of the suspended-dome structure.

The lateral stiffness of the support affects the far-end boundary conditions of the members connected to the unsupported nodes, and thus influences the stiffness characteristics f_k of the members connected to the unsupported nodes. If fixed hinged supports are used, the far-end boundary conditions can be simplified as hinged connections. If sliding supports are chosen for the suspended-dome structure, there are two cases: (1) If the initial failure

occurs within the outermost hoop, the cable–strut system of the outermost hoop can still maintain the structure's self-balancing system, and the far-end boundary conditions can still be calculated as hinged connections. In this case, the impact of support lateral stiffness on the structure is relatively small. (2) If the initial failure occurs in the outermost hoop cable, the lateral stiffness of the outermost hoop member alone cannot provide sufficient axial support for the far end of the outermost diagonal or radial members. In this case, only the bending stiffness of the diagonal or radial members comes into play, and their node-buckling calculation model changes to the one shown in Figure 14.

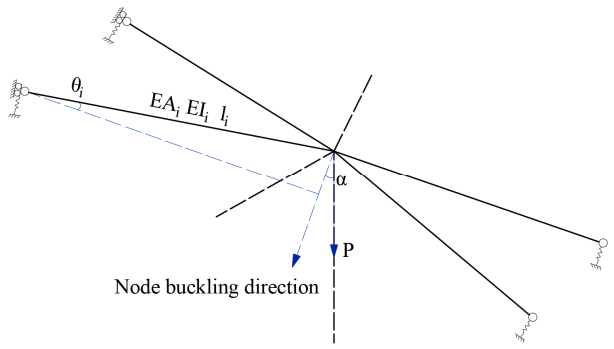

Figure 14. Node-buckling calculation model when using sliding supports.

Suppose there are n members connected to the unsupported node, among which m members are the outermost diagonal or radial members. Then, the weakening coefficient of the collapse bearing capacity of the structure using sliding supports is d_s, which can be expressed in the form of Equation (8).

$$\mathrm{d}_s = \frac{\sum_{i=1}^{n-m}\left(\frac{EA^i}{l^i}\sin^2(\theta^i) + \frac{3EI^i}{(l^i)^3}\cos^2(\theta^i)\right) + \sum_{i=1}^{m}\left(\frac{3EI^i}{(l^i)^3}\cos^2(\theta^i)\right)}{\sum_{\mathrm{i}=1}^{n}\left(\frac{EA^i}{l^i}\sin^2(\theta^i) + \frac{3EI^i}{(l^i)^3}\cos^2(\theta^i)\right)} \quad (8)$$

Taking the Kiewit suspended-dome structure model in Section 2.3 as an example, after the failure of the outer hoop cable, there are four diagonal members connected to the unsupported node J1-C3, of which two members are in the outermost area (i.e., n = 4, m = 2). When sliding supports are adopted, the weakening coefficient d_s is 0.58 according to Equation (8). This indicates that the sliding supports, compared to the fixed hinged supports, reduces the resistance index to 58% of its original value in the case of outer hoop-cable failure, demonstrating that the lateral stiffness of the supports has a significant impact on the collapse bearing capacity of suspended-dome structures.

FE analysis results can also verify this conclusion: the support J3-D1 is set as a fixed hinged support, while the radial displacement of the remaining support s is released, allowing them to slide freely. Additionally, the ring beams are added to ensure the load-bearing characteristics of the structure are consistent with the actual structure. The roof load also adopts G = 1.21 kN/m^2. The numerical simulation showed that progressive collapse occurred after the failure of the outer hoop-cable segment S1-C2, as shown in Figure 15.

Similar to Section 2.3, it can be seen from Figure 16a that the collapse sequence of the shell nodes was J1-C3—J1-B2—J2-C1—J2-B1—J2-A—JT, indicating that the structural failure began above the failed hoop-cable segment, and the local arch-like spatial grid centered on nodes J1-C2 and J1-C3 was still the first place to deform. At 1.6 s, buckling occurred at the outer hoop members, at 2.4 s, the local arch-like spatial grid had completely overturned, and at 3.2 s, the progressive collapse had extended to the middle and inner hoops.

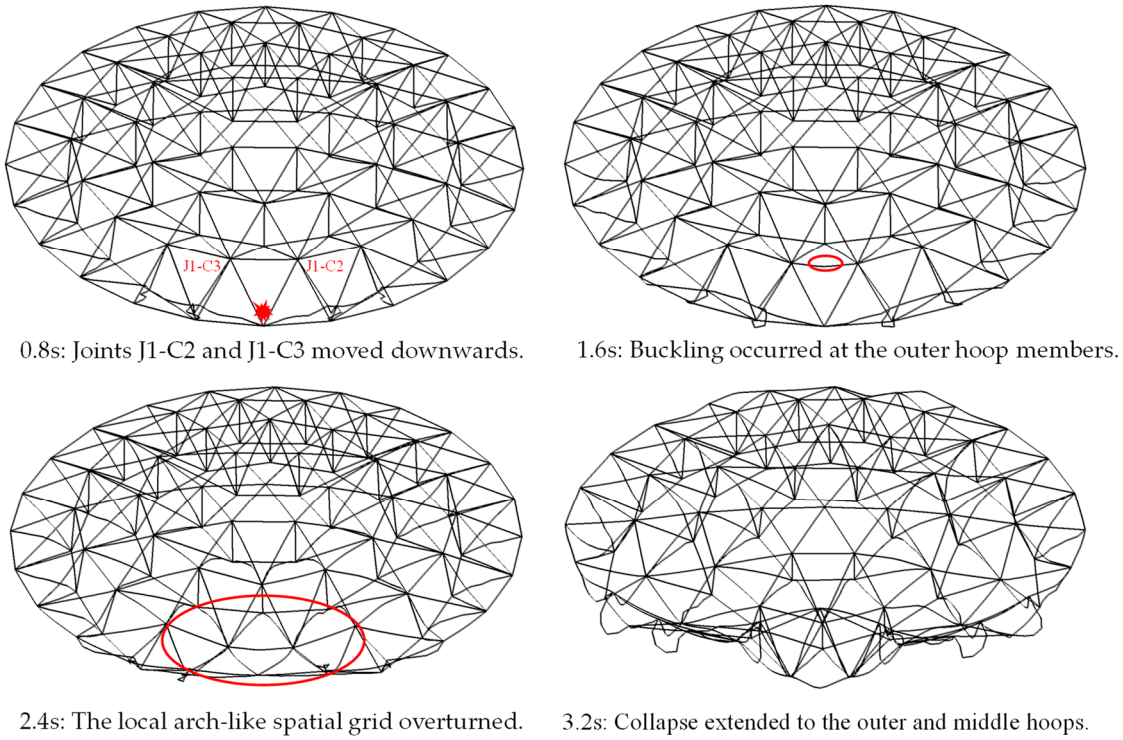

Figure 15. Collapse process of the suspended-dome structure with radial constraints released.

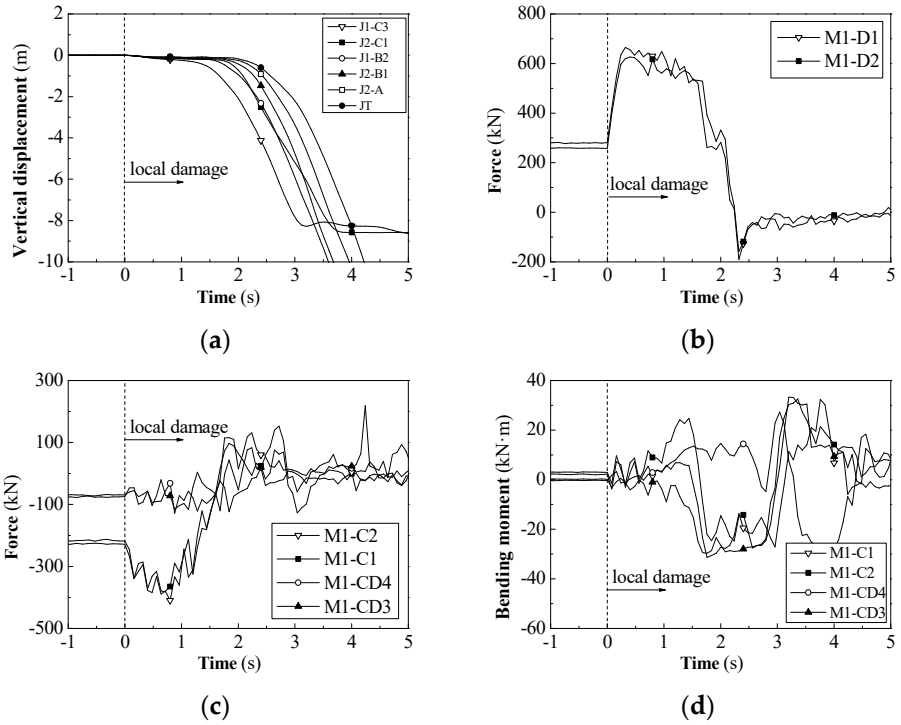

Figure 16. Time history of suspended-dome structures with radial constraints released. (**a**) Vertical displacement, (**b**) axial force in the ring beams, (**c**) axial force in the hoop and diagonal members, and (**d**) bending moment in the hoop and diagonal members.

Since the radial displacement was released at the supports, in the case of outer hoop-cable failure causing the self-balancing system to fail, the ring beams alone could not provide sufficient lateral stiffness to the local arch-like spatial grid, which was manifested as

a rapid transition of the axial force of the ring beams from tension to compression. As shown in Figure 16b, at 0.4 s, the axial tension of the ring beam (M1-D1 and M1-D2) increased rapidly, and then a transition from tension to compression occurred. The transition speed and the collapse of the local arch-like spatial grid were completely corresponding, reaching a compression peak of −191 kN at 2.4 s.

For the local arch-like spatial grid, the lack of sufficient lateral stiffness in the radial direction resulted in a severe weakening of the radial arch-mechanism, relying solely on the bending mechanism to resist external loads. This was manifested as a smaller increase in the axial force and a larger increase in the bending moment of the diagonal members at the outer hoop; while the hoop members still received the support of the remaining members of the shell, their loss of lateral stiffness was relatively small, and the arch-mechanism still played a role. This was manifested as a larger increase in the axial force of the circumferential members, and their axial compression rapidly increased from 220 kN to 420 kN within 0.8 s, as shown in Figure 16c. With the complete overturning of the local arch-like spatial grid, the axial forces of each member underwent a step-change from compression to tension. After the local arch-like spatial grid overturned, its collapse expansion process was the same as that in Section 2.3 and is not repeated here.

In summary, for suspended-dome structures with radial constraints released at the supports, when the outermost hoop cable fails, the weakening of lateral stiffness results in the destruction of the radial arch-mechanism of the local arch-like spatial grid, and the radial and diagonal members can only resist external loads by increasing the bending moment. This leads to the local arch-like spatial grid being unable to withstand external loads and causing a node-buckling phenomenon, which then extends to adjacent structures, causing the overall collapse of the structure.

6. Conclusions

In this study, the progressive-collapse mechanism of suspended-dome structures subjected to sudden cable rupture was proposed. The main results of this study were as follows.

(1) The progressive-collapse mechanism of suspended-dome structures after hoop-able failure can be summarized as follows: the failure of the hoop cable causes the corresponding upper lattice-shell nodes to lose the support of struts and become unsupported nodes. At this point, the unsupported nodes rely on the local arch-like spatial grid centered on themselves to resist external loads. Whether the local arch-like spatial grid can resist external loads through internal force redistribution will directly determine whether the overall structure undergoes progressive collapse. If the bearing capacity of the local arch-like spatial grid is higher than the external load, it can maintain balance by utilizing the arching and bending mechanisms. Once the bearing capacity of the local arch-like spatial grid is lower than the external load, node buckling similar to snap-through buckling will occur at the unsupported node, which is the direct cause of progressive collapse in suspended-dome structures.

(2) The node-buckling model and the calculation method of the resistance index are proposed: the node-buckling model focuses on a local arch-like spatial grid centered on unsupported nodes and takes into account the influence of the lower cable–strut system on the local arch-like spatial grid. The resistance index is formulated to quantitatively express the factors affecting the anti-collapse bearing capacity of suspended-dome structures.

(3) Using Ribbed and Lamella suspended domes as examples, the node-buckling model and resistance index are proven to be still applicable to and accurate for other types of suspended domes. The occurrence of node buckling in unsupported nodes directly precipitates the progressive collapse of the structure. A smaller resistance index implies a higher likelihood that the failure of a hoop-cable segment will trigger a progressive collapse within the structure.

(4) In addition to the structural rise–span ratio and the stiffness of the upper lattice-shell members, two factors that are easily overlooked—initial geometric imperfections and lateral stiffness at the supports—have a significant impact on the anti-collapse capacity. Initial geometric imperfections result in a rise–span ratio too small for the local arch-like spatial grid, while the lack of lateral stiffness at the supports will weaken the axial stiffness of the outermost radial or diagonal members. Both of these factors significantly reduce the stability of the local arch-like spatial grid, making it more likely to trigger progressive collapse in the suspended-dome structure. Hence, it is crucial to consider the influence of initial geometric imperfections and the type of supports when conducting a progressive-collapse analysis on actual suspended-dome structures.

As future work, it is recommended that comprehensive analysis methods are developed for the progressive collapse of suspended-dome structures, taking into account the initial geometric imperfections and the lateral stiffness of supports. These methods can be utilized for the practical analysis of the collapse resistance of suspended-dome structures. Furthermore, research on collapse-resistant design and recommendations should continue, aiming at enhancing the collapse redundancy of suspended-dome structures while considering economic efficiency and environmental sustainability. Lastly, given the critical role of steel cables in suspended-dome structures, it is crucial to implement damage monitoring and tension monitoring [17] for the cables. Further research can be conducted to investigate the effects of cable aging or relaxation on the performance of suspended-dome structures, ensuring their safety during service life.

Author Contributions: Conceptualization, S.Y.; methodology, S.Y.; software, Z.X.; validation, Z.X.; formal analysis, Z.X.; investigation, Z.X.; resources, S.Y.; data curation, Z.X.; writing—original draft preparation, Z.X.; writing—review and editing, S.Y. All authors have read and agreed to the published version of the manuscript.

Funding: The research was funded by the National Natural Science Foundation of China, grant number 51678432.

Data Availability Statement: The data presented in this study are available on request from the corresponding author.

Conflicts of Interest: The authors declare no conflict of interest.

References

1. GSA. *Progressive Collapse Analysis and Design Guidelines for New Federal Office Buildings and Major Modernization Projects*; General Services Administration: Washington, DC, USA, 2003.
2. JISF. *Guidelines for Collapse Control Design Construction of Steel Buildings with High Redundancy, Volume 1: Design*; Japan Iron and Steel Federation: Tokyo, Japan, 2005.
3. U.S. Department of Defense. *UFC 4-023-03 Design of Buildings to Resist Progressive Collapse*; U.S. Department of Defense: Washington, DC, USA, 2009.
4. *CECS 392—2014*; Code for Anti-Collapse Design of Building Structures. China Planning Press: Beijing, China, 2015.
5. Chen, Y.; Wang, L.; Yan, S.; Zhao, X. Study on the progressive collapse of large span truss-beam structures induced by initial member break. *IABSE Symp. Rep.* **2015**, *103*, 112–119.
6. Yan, S. Progressive Collapse Research of Large-Span Space Frame Structures. Ph.D. Thesis, Tongji University, Shanghai, China, 2015.
7. Zhao, X.; Yan, S.; Chen, Y.; Xu, Z. Experimental study on progressive collapse-resistant behavior of planar trusses. *Eng. Struct.* **2017**, *135*, 104–116. [CrossRef]
8. Zhao, X.; Yan, S.; Chen, Y. Comparison of progressive collapse resistance of single-layer latticed domes under different loadings. *J. Constr. Steel Res.* **2017**, *129*, 204–214. [CrossRef]
9. Yan, S.; Zhao, X.; Rasmussen, K.J.; Zhang, H. Identification of critical members for progressive collapse analysis of single-layer latticed domes. *Eng. Struct.* **2019**, *188*, 111–120. [CrossRef]
10. Tian, L.; Wei, J.; Huang, Q.; Ju, J. Collapse-resistant performance of long-span single-layer spatial grid structures subjected to equivalent sudden joint loads. *J. Struct. Eng.* **2021**, *147*, 04020309. [CrossRef]
11. Zhang, W.; Zhang, P. Numerical simulation of progressive collapse of suspended-dome structures. In Proceedings of the Twelfth National Conference on Modern Structural Engineering; Tianjin University: Tianjin, China, 2012; pp. 424–429.

12. Ou, T.; Chen, J.; Tan, J. Progressive collapse resistance analysis on conjoined suspendome structure of Zhaoqing new district stadium. *Build. Struct.* **2016**, *46*, 75–79.
13. Wang, X.; Chen, Z.; Yu, Y.; Liu, H. Numerical and experimental study on loaded suspendome subjected to sudden cable failure. *J. Constr. Steel Res.* **2017**, *137*, 358–371. [CrossRef]
14. Liu, R.; Zou, Y.; Wang, G.; Xue, S. On the Collapse Resistance of the Levy Type and the Loop-Free Suspen-Dome Structures After Accidental Failure of Cables. *Int. J. Steel Struct.* **2022**, *22*, 585–596. [CrossRef]
15. Zhao, X.; Xu, Z.; Yan, S. Experimental and numerical evaluation of structural performance of suspended-dome structures subjected to sudden cable rupture. *J. Constr. Steel Res.* **2023**. submitted.
16. ABAQUS Inc. *ABAQUS Release 6.13 Documentation*; ABAQUS Inc.: Palo Alto, CA, USA, 2013.
17. Khedmatgozar Dolati, S.; Caluk, N.; Mehrabi, A.; Khedmatgozar Dolati, S. Non-destructive testing applications for steel bridges. *Appl. Sci.* **2021**, *11*, 9757. [CrossRef]